Article

In vivo fluorescent ATP imaging of *Drosophila melanogaster* and *Caenorhabditis elegans* by using a genetically encoded fluorescent ATP biosensor optimized for low temperatures

Taiichi Tsuyama, Jun-ichi Kishikawa, Yong-Woon Han, Yoshie Harada, Asako Tsubouchi, Hiroyuki Noji, Akira Kakizuka, Ken Yokoyama, Tadashi Uemura, and Hiromi Imamura

Anal. Chem., **Just Accepted Manuscript** • DOI: 10.1021/ac4015325 • Publication Date (Web): 22 Jul 2013

In vivo fluorescent ATP imaging of *Drosophila melanogaster* and *Caenorhabditis elegans* by using a genetically encoded fluorescent ATP biosensor optimized for low temperatures

Taiichi Tsuyama[†,#], Jun-ichi Kishikawa[‡,#], Yong-Woon Han[¶], Yoshie Harada[†,¶], Asako Tsubouchi[†,‡‡], Hiroyuki Noji[††], Akira Kakizuka[†], Ken Yokoyama[‡], Tadashi Uemura[†], and Hiromi Imamura[†,¶,§,]*

[†]Graduate School of Biostudies, Kyoto University, Yoshida-Konoe-cho, Sakyo-ku, Kyoto 606-8501, Japan; [‡]Faculty of Life Sciences, Kyoto Sangyo University, Kamigamo-Motoyama, Kita-ku, Kyoto 603-8555, Japan;[¶]Institute for Integrated Cell-Material Sciences (WPI-iCeMS), Kyoto University, Yoshida-Honmachi, Sakyo-ku, Kyoto 606-8501, Japan; [††]Department of Applied Chemistry, The University of Tokyo, 7-3-1 Hongo, Bunkyo-ku, Tokyo 113-8501, Japan; [§]The Hakubi Center for Advanced Research, Kyoto University, Yoshida-Konoe-cho, Sakyo-ku, Kyoto 606-8501, Japan

ABSTRACT. Adenosine 5'-triphosphate (ATP) is the major energy currency of all living organisms. Despite its important functions, the spatio-temporal dynamics of ATP levels inside

living multi-cellular organisms is unclear. In this study, we modified the genetically encoded Förster resonance energy transfer (FRET)-based ATP biosensor ATeam to optimize its affinity at low temperatures. This new biosensor, AT1.03NL, detected ATP changes inside *Drosophila* S2 cells more sensitively than the original biosensor did, at 25°C. By expressing AT1.03NL in *Drosophila melanogaster* and *Caenorhabditis elegans*, we succeeded in imaging the *in vivo* ATP dynamics of these model animals at single-cell resolution.

Introduction

Genetically encoded fluorescent biosensors are powerful tools for visualizing spatio-temporal information in living cells[1-4]. These biosensors can be used in both cultured cells and multi-cellular organisms. Generally, genetically encoded fluorescent biosensors are designed for use in mammalian cells. Thus, modification or reconstruction of biosensors is sometimes required before use in non-mammalian model organisms. One major reason for this is that biosensors utilizing mammalian host-derived proteins sometimes do not work properly in heterologous systems. For example, the fluorescent cell-cycle biosensor Fucci utilizes 2 human proteins Geminin and Cdt1, which accumulate during the S/G2/M and G1 phases, respectively[5]. However, human Geminin and Cdt1 were replaced by those from other species when the biosensor was used in the fruit fly or zebra fish[6,7]. Another reason for modification that is less well known is that the properties of component proteins of biosensors, such as affinity towards ligands, change with temperature. We previously developed the genetically encoded fluorescent biosensors ATeams[8-10], which can be used to specifically monitor the levels of ATP, the major energy currency of cells. The dissociation constant (K_d) of an ATeam (AT1.03[8]) for mammalian

cells, which is approximately 3 mM at 37°C, decreases to approximately 0.6 mM at 25°C, which is far below the physiological ATP concentrations. Therefore, the FRET signal of the ATeam biosensor is mostly saturated at physiological concentrations of ATP and lower temperatures. Thus, it is difficult to detect slight changes of ATP levels in the widely used invertebrate model animals *Drosophila melanogaster* and *Caenorhabditis elegans*, whose body temperatures are close to their environmental temperatures, typically between 20°C and 25°C. In fact, we previously reported expression of the original AT1.03 biosensor in vulva cells of *C. elegans*, but were unable to monitor changes in ATP level *in vivo*[11].

Over the past decade, *D. melanogaster* and *C. elegans* have emerged as model systems for bioenergetics and metabolism studies examining carbohydrates, lipids, and sterol homeostasis, for example[12-15]. Their well-characterized genomes and powerful genetic tools available have revealed evolutionarily conserved molecular mechanisms of physiology. Most major metabolic pathways are evolutionarily well conserved; it has recently been shown that the same central metabolic regulators are found both in the invertebrate model animals described above and in mammals. A potential disadvantage of using the model animals in metabolism studies is their small body size, which makes applications of classical biochemical assays to specific cell types technically difficult or labor-intensive. Importantly, it has been reported that there is remarkable heterogeneity in metabolic activities and in susceptibilities to dysfunction of given metabolic pathways between tissues or cellular subtypes. For example, in mitochondrial bioenergetics, the amounts, activities, and control coefficient values of individual enzymes involved in oxidative phosphorylation (OXPHOS) show differences between tissues[16-18], and symptoms associated with mitochondrial diseases show cell-type specific expression[19-21]. Therefore, imaging techniques using genetically encoded fluorescent metabolite biosensors can be used to

circumvent difficulties in measuring metabolite levels in a small number of selective cell types within the larger tissue of model animals. Genetically encoded fluorescent biosensors for metabolites have been previously reported[8,22-26]; however, all are intended for use in mammalian cells.

Here, we report a modified ATeam biosensor that has been optimized for use at relatively low temperatures (20 to 30°C). This new biosensor, AT1.03NL, shows a larger dissociation constant than the original AT1.03 and maintains binding specificity to ATP and stability of FRET signals over a physiological pH range *in vitro*. We also showed that AT1.03NL can be used to detect changes in ATP concentration more sensitively than the original biosensor at 25°C in *Drosophila* S2 cells. Furthermore, we succeeded in imaging ATP dynamics inside whole-mount or fillet preparations of *D. melanogaster* and whole-mounts of *C. elegans* at single-cell resolution.

Experimental

Chemicals

ATP, adenosine 5'-diphosphate (ADP), 2-deoxyglucose (2DG), and oligomycin A were purchased from Sigma (St. Louis, MO, USA). Deoxynojirimycin and Antimycin A were purchased from Santa Cruz Biotech (Santa Cruz, CA, USA) and Enzo Life Sciences (Farmingdale, NY, USA). Guanosine 5'-triphosphate (GTP), uridine 5'-diphosphate (UTP), and cytosine 5'-triphosphate (CTP) were from Jena Biosciences (Jena, Germany). Nicotinamide adenine dinucleotide (NADH) was from Roche Applied Science (Basel, Switzerland). DNA polymerase and DNA ligation kits were from Takara (Shiga, Japan). Other chemical reagents were purchased from Wako Pure Chemicals (Osaka, Japan) or Nacalai Tesque (Kyoto, Japan), unless otherwise noted. ATP and other nucleotides (except NADH) were complexed with

equimolar $MgCl_2$ before use in the experiments; therefore, the term ATP in this study indicates MgATP.

Plasmids

εMet60-Leu and εLys132-Asn mutations were introduced into the pRSET-AT1.03 plasmid by using a PCR-based method to obtain pRSET-AT1.03NL plasmid. To express AT1.03NL and the original AT1.03 in S2 cells and flies, we used the Gal4-UAS system. pUAST-AT1.03, pUAST-AT1.03NL, and pUAST-AT1.03$^{R122K/R126K}$ (pUAST-AT1.03RK) plasmids were generated using standard cloning techniques.

The AT1.03NL expression plasmid for *C. elegans*, pPmyAT1.03NL, was constructed based on the vector pFX_DsRedXT[27]. The AT1.03NL gene was connected to the *myo-2* promoter, which promotes specific protein expression in pharyngeal muscle cells, using a PCR-based method. The AT1.03NL fragment was inserted into pFX_DsRedXT to exchange the coding sequence region of DsRed.

Expression and purification of ATeam biosensors

Escherichia coli strain JM109 (DE3) (Promega, Fitchburg, WI, USA) carrying pRSET-AT1.03 or pRSET-AT1.03NL was cultured in LB medium at 24°C for 24 h. Cells were collected by centrifugation, suspended in buffer A (100 mM sodium phosphate, pH 8.0; 200 mM sodium chloride; 10 mM imidazole-HCl), and then disrupted by sonication. After centrifugation, the supernatant was applied to a Ni-NTA column (Qiagen, Hilden, Germany) equilibrated with buffer A. After washing the column with buffer A, the protein was eluted by increasing the imidazole concentration to 200 mM. Fractions containing ATeam were concentrated and applied

to Superdex 200 gel-filtration columns (GE Healthcare, Little Chalfont, UK) equilibrated with 20 mM Tris-HCl (pH 8.0), 150 mM NaCl, and 1 mM EDTA-Na. After adding glycerol to a final concentration of 20% (w/v), the purified ATeam biosensors were stored at −80°C until use.

Measurement of fluorescence in vitro

The fluorescence of purified ATeam biosensors was investigated in a buffer containing 50 mM MOPS-KOH (pH 7.3), 50 mM KCl, 0.5 mM $MgCl_2$, and 0.05% (w/v) Triton X-100. MOPS-KOH (pH 6.5, 6.7, 6.9, 7.1, or 7.5) or HEPES-KOH (pH 7.7, 7.9, 8.1, or 8.3), rather than MOPS-KOH (pH 7.3), was used to investigate the effect of pH. To obtain the fluorescence spectra, mseCFP was excited at a wavelength of 435 nm and emission was observed from 460 to 600 nm was scanned using a FluoroMax4 spectrofluorometer (Horiba, Kyoto, Japan). To measure the kinetics of the YFP/CFP ratio change due to binding of ATP, CFP was excited using 435 ± 2.3 nm light and emission spectra at 480 ± 20 nm and 550 ± 40 nm were simultaneously monitored every 0.5 s using a SX20 stopped-flow spectrophotometer (Applied Photophysics, Surrey, UK). The time course of the ratio change was fitted to a single exponential equation to calculate the apparent rate of binding.

Culture and transfection of Drosophila *S2 cells*

S2 cells were cultured at 25°C in Schneider's *Drosophila* medium (Gibco, Grand Island, NY, USA) containing 10% fetal bovine serum (GIBCO) and penicillin/streptomycin, and passaged every 3 to 4 days. S2 cells were cotransfected with *pDA-Gal4* (actin-promoter Gal4; a gift from Fumio Matsuzaki's lab) and *pUAST-ATeams* by using HilyMax (Dojindo, Kumamoto, Japan), and used for microscopic analysis 3 days after transfection.

Transgenic Drosophila *stocks*

Fly stocks were maintained at 25°C on standard corn meal-agar-yeast food. We generated transgenic lines carrying *UAS-AT1.03NL* or *UAS-AT1.03RK* by germ-line transformation. *Gal4* driver strains used in this study included $Gal4^{109(2)80}$ (ref. 28), *Gal4-Mef2.R*, and *Ubi-Gal4* (Bloomington Stock Center).

Transient expression of AT1.03NL in C. elegans

Caenorhabditis elegans strain used in this study was derived from the wild-type Bristol strain N2, and was maintained using standard techniques[29]. To obtain worms expressing AT1.03NL, the expression plasmid was microinjected into the distal gonad of an adult hermaphrodite of *C. elegans*[29]. Transient lines were established and maintained by selection for their ATeam fluorescence in pharyngeal muscle. Resulting lines were used in the following experiments.

Luciferase-based ATP assay of C. elegans

Day 5 worms were transferred onto 2% agarose gel with or without 0.5% 1-phenoxy-2-propanol and incubated for 50 min. Next, each worm was transferred into 50 µL S-basal (50 mM NaPi, 0.1 M NaCl, pH 6.0) in 1.5-mL tubes. The tubes were flash-frozen in liquid nitrogen and then boiled for 10 min. After centrifugation (15,000 ×*g*, 10 min), the supernatant solution was subjected to ATP measurement by using a luciferin/luciferase assay kit (CellTiter-Glo™, Promega).

Imaging

Transfected S2 cells were seeded onto concanavalin-A-coated glass-bottomed culture dishes (IWAKI) and incubated for 8 to 12 h before observation. For live imaging of fly larvae, late third instar larvae (~120 h after laying an egg) were collected and dissected in Hemolymph-like 6 (HL6) medium. HL6 medium contains 80 mM trehalose as an energy substrate[30]. To obtain ATeam1.03NL signals in muscles, larvae were pinned to and dissected on Sylgard 184 (Corning, Corning, NY, USA)-coated glass-bottomed dishes, and time-lapse recordings were performed through the Sylgard layer (Fig. 7A–C). For the data collection of Fig. 7D, the larvae were dissected on Sylgard, treated with drugs for 2 h, and then placed under cover glasses. To inhibit muscle contractions, we added 7 mM L-glutamate to HL6 medium[31], and removed central nervous systems containing cell bodies of motor neurons. For *ex vivo* imaging for salivary glands, salivary glands were dissected out of larvae and mounted in HL6 medium on Sylgard-coated glass-bottomed dishes. The glands were observed through the Sylgard layer. For imaging of peripheral sensory neurons, a method involving a magnet chamber was performed essentially as described previously[32]. S2 cells and fly tissues were maintained at 25°C during experiments. S2 cells and fly larvae were viewed by using a laser scanning confocal microscope (Ti-E inverted microscope with a C1 confocal unit, Nikon, Tokyo, Japan) that was equipped with a 440 nm solid-state laser (Melles Griot, Albuquerque, NM, USA). Dual-emission ratio imaging of ATeams was performed using a 480dclp dichroic mirror and 2 emission filters (HQ450/35 for CFP and HQ515/30 for YFP-FRET), which were purchased from Chroma Technology Corp., Bellows Falls, VT, USA). The following objective lenses from Nikon were used: PlanApo VC 20× numerical aperture (NA) 0.75 (Fig. 4, 5A, 6, and 7), PlanFluor 40× NA 1.30 (Fig. 5B and C), and PlanApo VC 10× NA 0.45 (Fig. 5D). A series of z-sections was projected when necessary.

For imaging of *C. elegans*, transient worms were synchronized by the bleaching method[33]. Day 5 worms were mounted on a coverslip coated with agarose, which was covered with agarose gel (thickness ≈ 1 mm) containing 0.5% 1-phenoxy-2-propanol. Fluorescent imaging was performed after the worm had nearly stopped moving on a Nikon Ti-E-PFS inverted microscope (Nikon) by using a PlanApoVC ×20, 0.75 numerical aperture (NA), dry objective lens (Nikon). Filters used for dual-emission ratio imaging of ATeam were purchased from Semrock (Rochester, NY, USA): an FF02-438/24 excitation filter, an FF458-Di01 dichroic mirror, and 2 emission filters (FF01-483/32 for CFP and FF01-542/27 for YFP). Two emission filters were alternated by using a filter changer (Nikon). Worms were illuminated using a 75-W xenon lamp through 12.5% and 25% neutral density filters. Fluorescence emission from ATeam was imaged using a cooled charge-coupled device (CCD) camera (ORCA-AG; Hamamatsu Photonics, Tokyo, Japan); the exposure times were 300 ms for CFP and YFP-FRET images. Worms were maintained on a microscope at 25°C.

Image analyses for *D. melanogaster* and *C. elegans* were performed using EZ-C1 (Nikon) and MetaMorph (Molecular Devices, Carlsbad, CA, USA), respectively. Briefly, after background subtraction from CFP and YFP-FRET images, mean intensities of CFP and YFP-FRET emissions within a region-of-interest (ROI) were separately calculated. The YFP-FRET/CFP emission ratio was calculated by dividing mean intensity of YFP-FRET emission with that of CFP emission in ROI. Ratio images are shown by intensity modulated display (IMD) by using MetaMorph.

Results and Discussion

Development of a new ATeam biosensor optimized for low temperature

The ε subunit, an ATP-sensing part of ATeam biosensor, undergoes large conformational changes upon binding of ATP (Fig. 1). Nuclear magnetic resonance studies have shown that the C-terminal domain (CTD) of ε subunit has extended and fluctuating conformations in the absence of ATP, but fixes into a closed conformation when ATP binds to ε[34]. According to X-ray structure analysis, the interaction between NTD and CTD contributes to the closed conformation of the ATP-bound form[34]. Because K_d for ATP is determined by the equilibrium between ATP-bound (closed) and ATP-free (extended) forms, destabilization of ATP-bound form was expected to increase the K_d of ε.

We introduced mutations at a position 60 from NTD and a position 132 from CTD, which interacts in the crystal structure to destabilize the closed form. Among the number of mutants investigated, we found that a mutant AT1.03 biosensor with Met60Asn and Lys132Leu mutations (abbreviated as AT1.03NL) was adequate for use at low temperature. The FRET signal (FRET/CFP emission ratio) of AT1.03NL increased by 99 ± 15% (mean ± SD, n =3; as assessed by the emission ratio of 527/475 nm) upon the addition of ATP *in vitro* (Fig. 2A). This AT1.03NL showed K_d for ATP of 1.77 ± 0.33 mM (mean ± SD, n = 3) at 24°C, while K_d of the original AT1.03 was 0.64 ± 0.05 mM (mean ± SD, n = 3) (Fig. 2B). At all temperature range tested (20 to 30°C), AT1.03NL showed approximately 3-fold higher K_d values than AT1.03. Even at 20°C, the K_d of AT1.03NL exceeded 1 mM. To investigate whether the increase of K_d by M60N/K132L mutations is caused by decrease in k_{on} or increase in k_{off}, or both, we analyzed the kinetics of 2 biosensors by using a stopped-flow fluorometer at 24°C (Fig. 2C). It was observed that both decreased k_{on} for ATP ($7.5 \pm 1.2 \times 10^{-3}$ mM^{-1} s^{-1}) and increased k_{off} ($2.9 \pm 0.2 \times 10^{-2}$ s^{-1}) of AT1.03NL (mean ± SD, n = 3) as compared to AT1.03 ($k_{on} = 3.0 \pm 0.4 \times 10^{-2}$ mM^{-1} s^{-1}; $k_{off} = 1.32 \pm 0.02 \times 10^{-2}$ s^{-1}; mean ± SD, n =3) contributed to lower ATP affinity (Fig. 2C).

Next, we tested whether the mutant possessed high selectivity to ATP. As shown in Fig. 3A, the FRET signal of AT1.03NL did not increase because of ADP, GTP, UTP, CTP, or NADH, indicating that the signal will not be affected by changes of other related nucleotides. The FRET signal was almost unaffected by pH between 6.9 and 8.3 (Fig. 3B), indicating that fluctuation around physiological pH in the cytoplasm and mitochondria will have only small effects on the FRET signal of AT1.03NL.

Evaluation of the new ATeam biosensor in Drosophila *S2 cells*

To examine whether AT1.03NL works better than AT1.03 in a cellular system at low temperatures, we used cultured S2 cell line derived from *D. melanogaster*, which is normally grown at 25°C. Either AT1.03 or AT1.03NL was expressed in S2 cells. Expressed biosensors localized to cytoplasm according to fluorescence microscopy results (Fig. 4A). We predicted that the FRET signal of AT1.03 is nearly saturated in the cells at normal conditions and responds slowly to changes in the ATP level.

We investigated how the FRET signal of AT1.03- or AT1.03NL-expressing cells changed when treated with 2DG and oligomycin A (OM), inhibitors for glycolysis and OXPHOS, respectively. Consistent with our prediction, a fraction of cells expressing AT1.03 showed slowly decreasing fluorescence emission ratio, whereas such a fraction showing slow responses was rarely observed in cells expressing AT1.03NL (Fig. 4B). Quantitatively, the populations of AT1.03-expressing cells that showed FRET signals of greater than 2.0 (in the ratio) after 15 and 30 min of the inhibitor treatment were 38 and 29%, respectively, whereas those of AT1.03NL-expressing cells were only 9 and 1%, respectively (Fig. 4C). In addition, most AT1.03NL cells showed a higher initial rate in FRET signal change after metabolic challenge (Fig. 4D). As a negative

control, we also expressed AT1.03$^{R122K/R126K}$ (abbreviated as AT1.03RK hereafter), which has a very low affinity to ATP and cannot respond to changes in physiological ATP level *in vitro*[8]. The FRET signal of AT1.03RK was much lower throughout our monitoring and did not alter in the presence of inhibitors (Fig. 4E). Collectively, AT1.03NL is superior to the original AT1.03 at a low temperature in S2 cells.

Ex vivo *and* in vivo *ATP imaging of D. melanogaster larvae*

To detect changes in ATP concentration in live animals, we used the *Drosophila* Gal4-UAS system and expressed AT1.03NL or AT1.03RK in various cell types. When we observed multi-dendritic sensory neurons (md neurons)[28], fluorescence emission ratios of individual neuronal cell bodies were measured (Fig. 5A–5C). High-level expression of such biosensors *in vivo* may perturb related cellular pathways by chelating endogenous functional molecules, which may be toxic for organisms. We strongly and broadly expressed AT1.03NL by using drivers such as *Ubi-Gal4* (Fig. 6) and *Gal4-Mef2.R* (Fig. 5D and 7). *Ubi-Gal4* is a fusion gene of the *ubiquitin* promoter and *Gal4*, which broadly drives transgene expression, whereas *Gal4-Mef2.R* composed of somatic, visceral, and cardiac regulatory elements of *Mef2*, selectively drives expression in muscles[35]. In either genetic condition, adult flies were viable, fertile, and morphologically normal (data not shown), suggesting that AT1.03NL expression did not impair normal development. These results are consistent with the fact that the cellular concentration of ATP is in the millimolar range and far higher than that of cellular proteins.

Next, we attempted to verify whether fluorescence emission ratios of AT1.03NL represented the change in intracellular ATP level in tissues. For this purpose, we examined effects of applying OXPHOS inhibitors either on salivary glands that had been dissected from mature

larvae (Fig. 6) or on body wall muscles in larval fillet preparations (Fig. 7). The emission ratios of salivary glands rapidly decreased upon application of antimycin A (AM), which inhibits OXPHOS complex III, or OM that inhibits complex V, and the ratio was ceased decreasing 20 min after addition (Fig. 6A–C). In contrast, ratios of AT1.03RK remained low (Fig. 6D). These results suggest that the FRET signal of AT1.03NL is dependent on its binding to ATP and that ATP concentration was below the limit of detection 20 min after AM addition.

Compared to the FRET signal in the salivary glands, the emission ratios in the body wall muscles decreased significantly more slowly or did not decrease significantly following the application of the OXPHOS inhibitors tested (AM, OM, KCN, or AM plus KCN) (Fig. 7A–D). These results suggest that the cellular ATP level in muscle is maintained in at least the millimolar range for 2 h in the presence of OXPHOS inhibitors. We suspected that the slow reduction in the ratio in the muscle implies a supply of ATP from another metabolic pathway (i.e., glycolysis). Consistently, simultaneous inhibition of OXPHOS and the glycolytic flux by applying deoxyglucose (2DG) and deoxynojirimycin, an inhibitor of trehalase (a glucosidase of trehalose, a major energy substrate in hemolymph of *Drosophila*)[36], together with AM caused a more rapid decrease in the signal (Fig. 7C and D). These results suggest that glycolytic activity in body wall muscles is higher than that in the salivary glands when OXPHOS is blocked.

In vivo ATP imaging of *Caenorhabditis elegans*

Several lines of evidence suggest that anesthetics can impede mitochondrial function or destroy mitochondrial structures[37-41]. However, it remains unclear whether anesthetics can affect intracellular ATP levels *in vivo*. In this study, we transiently expressed AT1.03NL in pharyngeal muscle cells of *C. elegans* by using the myosin promoter (Fig. 8A) and investigated the effect of

the anesthetic on intracellular ATP levels. We treated worms with an anesthetic reagent, 1-phenoxy-2-propanol (PP), a commonly used anesthetic for *C. elegans*. During anesthetization of *C. elegans*, we found that the ATP level inside pharyngeal muscle gradually declined (Fig. 8A and B). ATP levels were nearly depleted within 50 min after treatment with PP in 7 worms out of 10 that were investigated (Fig. 8B). PP did not alter fluorescent spectrum of AT1.03NL *in vitro* (data not shown). Although the worms stopped moving before ATP levels of pharyngeal muscle began to decline, ATP levels of cells required for locomotion, such as motor neuron, may have decreased much earlier. ATP level of whole worms, which was measured by a traditional firefly luciferase assay, was also decreased by PP (Fig. 8C). The ATP decline was, however, much smaller than expected from ATP imaging of pharyngeal muscle. The effect of PP might only appear in some part of body. Our results suggest that the anesthetic can reduce intracellular ATP level, likely by inhibiting mitochondrial functions. Caution should be used when interpreting metabolism data when anesthetics are used, since changes in ATP level could largely affect various metabolic pathways.

Conclusions

A new variant of a genetically encoded FRET-based ATP biosensor, AT1.03NL, showed a K_d value appropriate for use at low temperatures in aqueous solution. The superiority of this new variant at low temperatures over the original biosensor was confirmed by imaging intracellular ATP in *Drosophila* S2 cells. Finally, *ex vivo* and *in vivo* ATP imaging of *D. melanogaster* and *C. elegans* performed using AT1.03NL allowed the monitoring of dynamics of intracellular ATP levels in tissue and living organisms.

Intracellular ATP is utilized for many basic cellular activities, including protein synthesis and degradation, metabolic reactions, membrane transport, and intracellular trafficking. There is growing evidence from genetic studies of model organisms, including *D. melanogaster* and *C. elegans*, that energy metabolism is involved in diverse complex biological processes that are required for the development and maintenance of individual tissues. For example, mitochondrial biogenesis and localization is involved in the formation of neuronal dendritic spines[42,43], and mitochondrial dysfunction affects morphology of dendritic arbors[44,45]. Furthermore, bioenergetics plays important roles during epithelial cell polarization[46,47]. Studies of model organisms also revealed energy metabolism may be related to aging[48-52], and some enzymes involved in energy metabolism are required for non-apoptotic cell death[53]. The *in vivo* ATP imaging method described here can be used to investigate differences in energy metabolism in model animals with various genetic backgrounds at single-cell resolution. This will allow further understanding of the connection between energy metabolism and complex biological processes.

FIGURES.

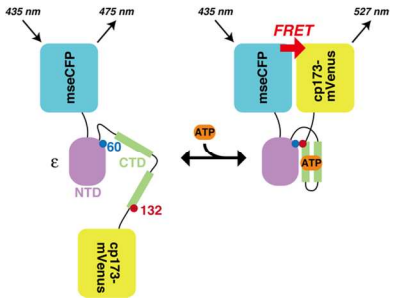

Figure 1. Schematic drawing of ATeam biosensor

ATeam biosensor changes its conformation from open state (left) to closed state (right) by binding ATP. This conformational change enhances FRET from CFP (mseCFP) to YFP (cp173-

mVenus). Positions of 60th and 132nd resides are indicated by blue and red circles, respectively. NTD, N-terminal domain of ε subunit; CTD, C-terminal domain of ε subunit.

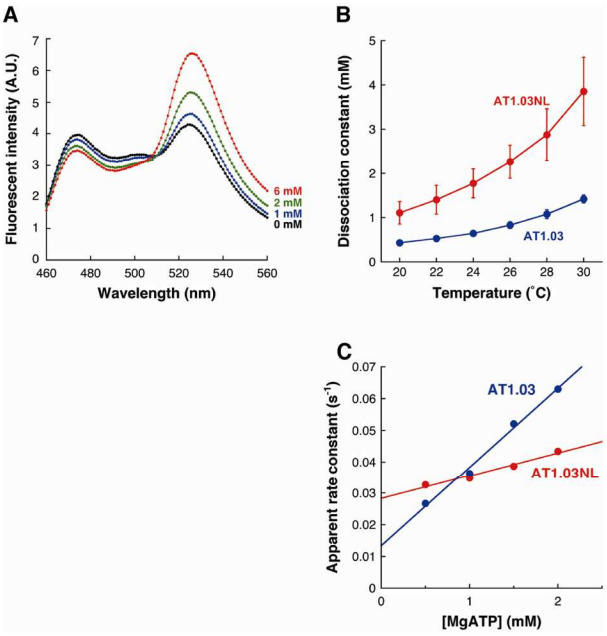

Figure 2. New AT1.03NL biosensor optimized for low temperatures

(A) Fluorescence emission spectra of AT1.03NL. Black, 0 mM; blue, 1 mM; green, 2 mM; red, 6 mM MgATP. (B) Dependence of K_d on temperature. K_d values (mean ± SD, n = 3) of AT1.03 (blue) and AT1.03NL (red) were determined at 20, 22, 24, 26, 28, and 30°C as described previously[8]. (C) Kinetic analysis of AT1.03 and AT1.03NL. Apparent rate constants (k^{app} = k_{on}[ATP] + k_{off}) at 24°C, which were determined by fitting the FRET signal increase after ATP addition with a single exponential equation, were plotted against [ATP]. Slope and y-intercept of a linear fitting represent k_{on} and k_{off}, respectively. Blue, AT1.03; red, AT1.03NL. One representative plot is shown (n = 3).

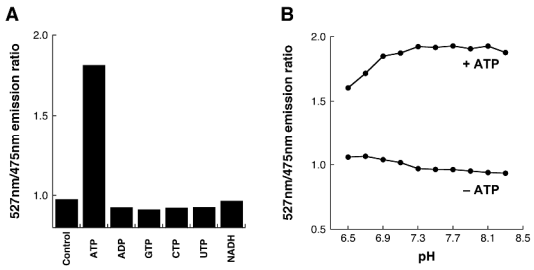

Figure 3. *In vitro* properties of AT1.03NL

(A) Nucleotide selectivity of AT1.03NL. The FRET signal of AT1.03NL at 24°C in the presence of 5 mM of the indicated nucleotide is shown. Mean values from two independent experiments are shown. (B) pH dependence of AT1.03NL. The FRET signal at 24°C in the absence or presence (6 mM) of ATP over the pH range of 6.5–8.3 is shown. Mean values from two independent experiments are shown.

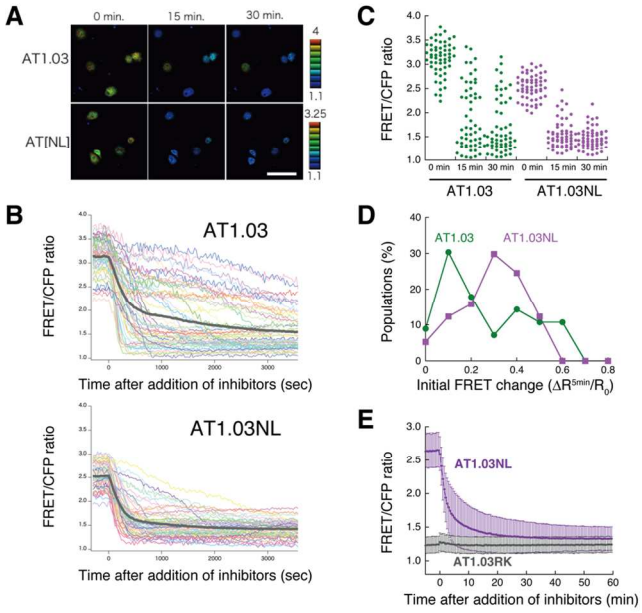

Figure 4. Evaluation of ATeam biosensors in *Drosophila* S2 cells

(A) Ratiometric pseudocolor images of S2 cells expressing AT1.03 (top) or AT1.03NL (bottom). Elapsed time (in min) after the addition of the inhibitors (50 mM 2-deoxyglucose and 20 μM of oligomycin) is shown at the top left of the cells. Scale bar: 5 μm. (B-D) Comparisons of the effects of inhibitors on fluorescence emission ratios of AT1.03 and AT1.03NL in S2 cells (n > 60 cells for each ATeam transfection). (B) Time courses of emission ratios of the S2 cells expressing AT1.03 (top) or AT1.03NL (bottom). Ratios of individual S2 cells are indicated as different color lines; averages are dark thick lines. Inhibitors were added at time 0 (min). (C and D) Distributions of emission ratios at indicated time points (C) and initial (5 min after addition of the inhibitors) ratio changes (D) of S2 cells expressing AT1.03 (green) or AT1.03NL (magenta). (E) Time courses of average ratios of S2 cells expressing AT1.03NL (magenta, n = 31) or AT1.03RK (gray, n = 27) that had been treated with 2-deoxyglucose (2DG) and oligomycin (OM). Error bars indicate standard deviations.

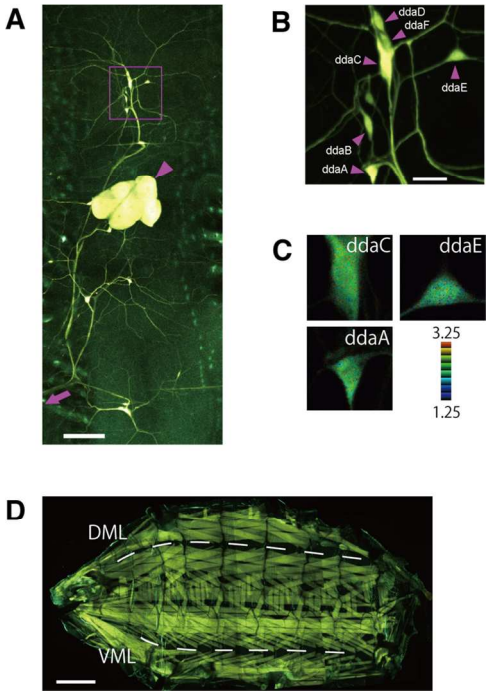

Figure 5. Expression of AT1.03NL in *Drosophila melanogaster*

(A and B) Fluorescent image of an abdominal hemisegment of a fillet preparation of a larva expressing AT1.03NL. (A) AT1.03NL was expressed in multi-dendritic (md) neurons and oenocytes (arrowhead). Axons of md neurons extended towards the ventral central nervous system (arrow). Axons and dendrites of md neurons were visualized and a high-power image of the boxed region is indicated in "B." (B) Dorsal cluster of sensory neurons. Cell bodies of identified md neurons are marked (arrowheads). (C) Fluorescent emission ratio image of cell bodies of md neurons in "B." Anterior is to the left and dorsal is up in "A"–"C," Fig. 7A, and 7B. (D) Fluorescent images of body wall muscles of a dissected larva expressing AT1.03NL. DML and VML indicate dorsal midline and ventral midline, respectively. Scale bars: 100 μm (A), 20 μm (B), 500 μm (D). Genotypes: (A–C) *Gal4*$^{109(2)80}$ *UAS-ATeam1.03NL*/+ and (D) *Mef2-Gal4 UAS-ATeam1.03NL*/+.

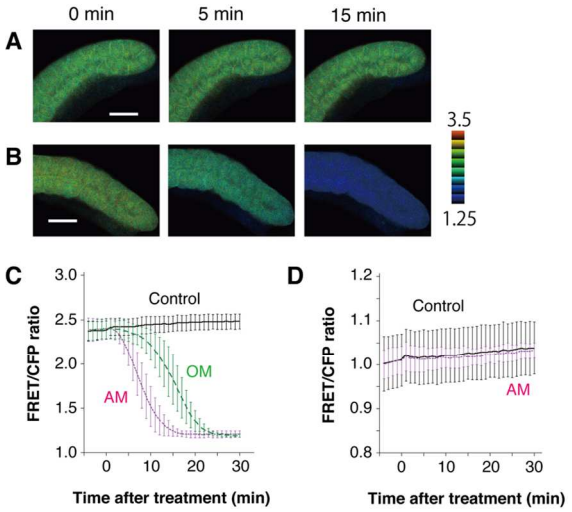

Figure 6. *Ex vivo* ATP imaging of *Drosophila* salivary glands

(A, B) Ratiometric pseudocolor images of *ex vivo* salivary glands expressing AT1.03NL. Salivary glands were dissected out of mature third instar larvae and treated with DMSO (A) or 20 μM antimycin (AM; B). Elapsed time after the addition of the inhibitor is indicated. Scale bar: 100 μm. (C and D) Time courses of average ratios of AT1.03NL (C) or AT1.03RK (D) expressing salivary glands that were treated with either DMSO (control), 20 μM AM, or 50 μM oligomycin (OM). The number of glands assayed was 7 (DMSO), 6 (AM), or 6 (OM). Error bars indicate standard deviations. Genotype: (A–C) *Ubi-Gal4 UAS-AT1.03NL*/+ and (D) *Ubi-Gal4 UAS-A 1.03RK*/+.

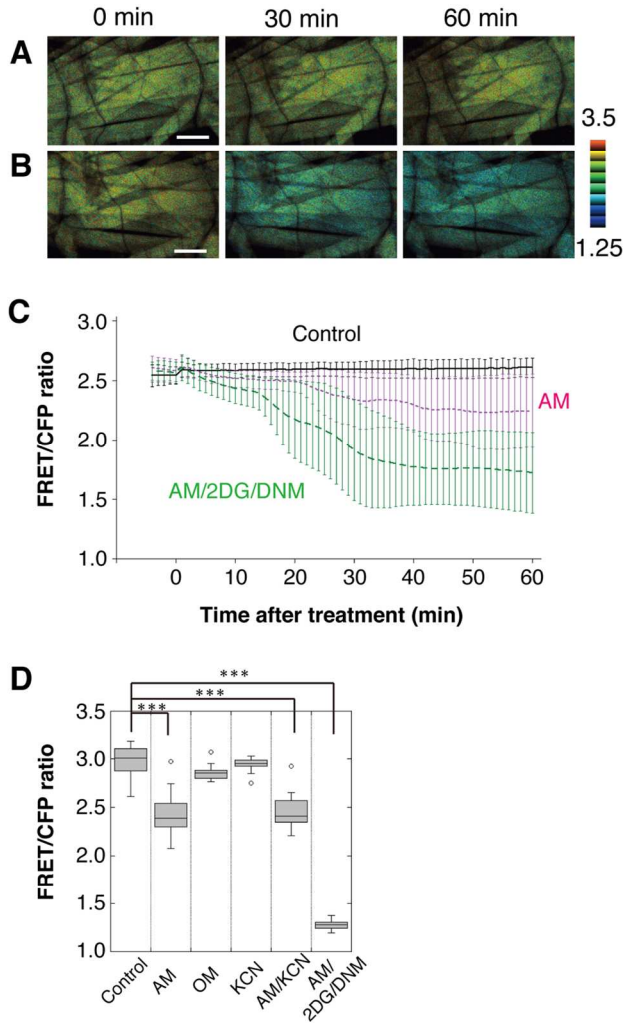

Figure 7. *In vivo* ATP imaging of *Drosophila* body-wall muscles

(A, B) Ratiometric pseudocolor images of body-wall muscles expressing AT1.03NL, A mature third instar larva was dissected and treated with DMSO (A) or a mixture of inhibitors (B), which included 100 µM AM, 50 mM deoxyglucose (2DG) and 100 µM deoxynojirimycin (DNM) (B). Images of the ventral portions of abdominal segments 4. Scale bar: 100 µm. (C) Time course of fluorescent emission ratios of AT1.03NL treated with DMSO (control), AM, or AM+2DG+DNM. Error bars are standard deviations. (D) Box–and-whisker plots of ratios of AT1.03NL expressed in the muscles at 2 h after addition of with DMSO (Control; n = 17), AM (n = 13), OM (n = 17), KCN (n = 19), AM+KCN (n = 12), or AM+2DG+DNM (n = 11). n indicates

the number of larvae assayed. The bottom and top edges of each box indicate the 25th and 75th percentiles, respectively; the line indicates the median value; whiskers indicate the minimum and maximum values that were not considered outliers. ***: P > 0.001 (ANOVA with post-hoc Dunnett's test). Genotype: (A–D) *Mef2-Gal4 UAS-AT1.03NL*/+.

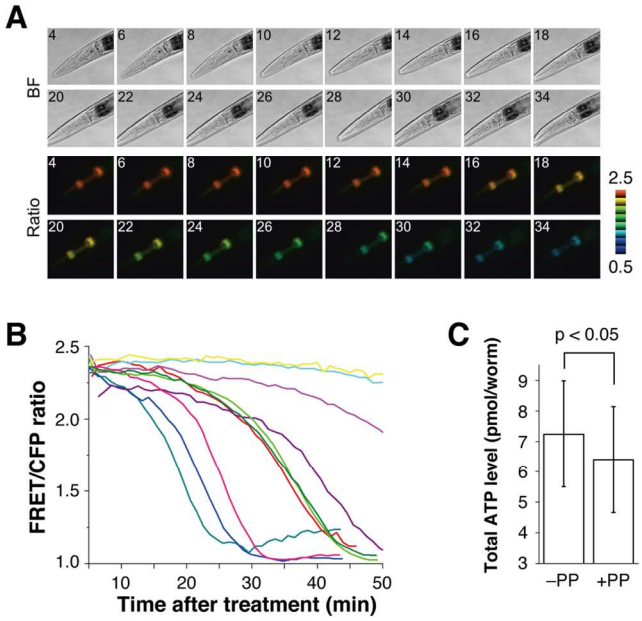

Figure 8. *In vivo* ATP imaging of *C. elegans* pharyngeal muscle cells

(A) Sequential images of bright-field (BF) and YFP/CFP emission ratio (Ratio, pseudcolored) of *C. elegans* expressing AT1.03NL treated with 1-phenoxy-2-propanol. Elapsed time (in min) after exposed to PP is shown at left side of the images. Images were obtained at 25°C (B) Time course of FRET/CFP ratio of AT1.03NL after treatment with PP. Each line was indicated by different color. (C) The effect of PP on ATP amount in each worm. ATP levels were measured after treatment with or without PP using a luciferin/luciferase assay (n = 29 and 24, respectively). Difference between groups was evaluated by t-test. Error bars represent the standard deviation.

AUTHOR INFORMATION

Corresponding Author

*Hiromi Imamura, Graduate School of Biostudies, Kyoto University, Yoshida-konoe-cho, Sakyo-ku, Kyoto 606-8501, Japan. E-mail; imamura@lif.kyoto-u.ac.jp.

Present Addresses

‡‡Department of Anesthesiology, Department of Cell Biology, and Department of Neurobiology, Duke University Medical Center, Durham, NC 27710, USA

Author Contributions

#These authors contributed equally.

Notes

ACKNOWLEDGMENT

Fly stocks were provided by the *Drosophila* Genetic Resource Center at Kyoto Institute of Technology and the Bloomington Stock Center. We also thank Kieta Nishida, Mayumi Futamata, Kumiko Shimizu, Junko Mizukoshi, and Kanae Oki for their technical assistance, and Yuriko Higuchi and Mitsuru Hashida for providing us with a spectrofluorometer. This work was supported in part by Grant-in-Aid for Young Scientists (22687011 to H. I.), by Grant-in-Aid for Scientific Research (A) (22247034 to T. U.), by a grant from the programs Grants-in-Aid for Scientific Research on Innovative Areas “Mesoscopic neurocircuitry” (22115006 to T. U.), and by Platform for Dynamic Approaches to Living System. T. T. was a recipient of a fellowship of the Japan Society for the Promotion of Science.

REFERENCES

(1) Miyawaki, A. *Dev Cell* 2003, *4*, 295.

(2) Palmer, A. E.; Qin, Y.; Park, J. G.; McCombs, J. E. *Trends Biotechnol* 2011, *29*, 144.

(3) Lalonde, S.; Ehrhardt, D. W.; Frommer, W. B. *Curr Opin Plant Biol* 2005, *8*, 574.

(4) Liemburg-Apers, D.; Imamura, H.; Forkink, M.; Nooteboom, M.; Swarts, H.; Brock, R.; Smeitink, J.; Willems, P.; Koopman, W. *Pharm Res* 2011, *28*, 2745.

(5) Sakaue-Sawano, A.; Kurokawa, H.; Morimura, T.; Hanyu, A.; Hama, H.; Osawa, H.; Kashiwagi, S.; Fukami, K.; Miyata, T.; Miyoshi, H.; Imamura, T.; Ogawa, M.; Masai, H.; Miyawaki, A. *Cell* 2008, *132*, 487.

(6) Nakajima, Y.; Kuranaga, E.; Sugimura, K.; Miyawaki, A.; Miura, M. *Mol Cell Biol* 2011, *31*, 2499.

(7) Sugiyama, M.; Sakaue-Sawano, A.; Iimura, T.; Fukami, K.; Kitaguchi, T.; Kawakami, K.; Okamoto, H.; Higashijima, S.; Miyawaki, A. *Proc Natl Acad Sci U S A* 2009, *106*, 20812.

(8) Imamura, H.; Nhat, K.; Togawa, H.; Saito, K.; Iino, R.; Kato-Yamada, Y.; Nagai, T.; Noji, H. *Proc Natl Acad Sci U S A* 2009, *106*, 15651.

(9) Kotera, I.; Iwasaki, T.; Imamura, H.; Noji, H.; Nagai, T. *ACS Chem Biol* 2010, *5*, 215.

(10) Nakano, M.; Imamura, H.; Nagai, T.; Noji, H. *ACS Chem Biol* 2011, *6*, 709.

(11) Kishikawa, J.; Fujikawa, M.; Imamura, H.; Yasuda, K.; Noji, H.; Ishii, N.; Mitani, S.; Yokoyama, K. *Microsc Res Tech* 2011, *75*, 15.

(12) Baker, K.; Thummel, C. *Cell Metab* 2007, *6*, 257.

(13) Niwa, R.; Niwa, Y. *Cholesterol* 2011, *2011*, 1.

(14) Harrison, J.; Haddad, G. *Annu Rev Physiol* 2011, *73*, 95.

(15) Schlegel, A.; Stainier, D. *PLoS Genet* 2007, *3*, e199.

(16) Fernandez-Vizarra, E.; Enríquez, J. A.; Pérez-Martos, A.; Montoya, J.; Fernández-Silva, P. *Mitochondrion* 2011, *11*, 207.

(17) Benard, G.; Faustin, B.; Passerieux, E.; Galinier, A.; Rocher, C.; Bellance, N.; Delage, J. P.; Casteilla, L.; Letellier, T.; Rossignol, R. *Am J Physiol Cell Physiol* 2006, *291*, C1172.

(18) Rossignol, R.; Letellier, T.; Malgat, M.; Rocher, C.; Mazat, J. P. *Biochem J* 2000, *347 Pt 1*, 45.

(19) DiMauro, S.; Schon, E. A. *N Engl J Med* 2003, *348*, 2656.

(20) Koopman, W.; Willems, P.; Smeitink, J. *N Engl J Med* 2012, *366*, 1132.

(21) Wallace, D. *Cold Spring Harb Symp Quant Biol* 2011, *76*, 1.

(22) Fehr, M.; Lalonde, S.; Lager, I.; Wolff, M.; Frommer, W. *J Biol Chem* 2003, *278*, 19127.

(23) Berg, J.; Hung, Y.; Yellen, G. *Nat Methods* 2009, *6*, 161.

(24) Zhao, Y.; Jin, J.; Hu, Q.; Zhou, H.; Yi, J.; Yu, Z.; Xu, L.; Wang, X.; Yang, Y.; Loscalzo, J. *Cell Metab* 2011, *14*, 555.

(25) Hung, Y.; Albeck, J.; Tantama, M.; Yellen, G. *Cell Metab* 2011, *14*, 545.

(26) San Martin, A.; Ceballo, S.; Ruminot, I.; Lerchundi, R.; Frommer, W. B.; Barros, L. F. *PloS ONE* 2013, *8*, e57712.

(27) Izumikawa, T.; Kitagawa, H.; Mizuguchi, S.; Nomura, K. H.; Nomura, K.; Tamura, J.; Gengyo-Ando, K.; Mitani, S.; Sugahara, K. *J Biol Chem* 2004, *279*, 53755.

(28) Grueber, W.; Jan, L.; Jan, Y. *Development* 2002, *129*, 2867.

(29) Evans, T. In *WormBook : The online review of C. elegans biology*; The *C. elegans* Research Community Ed. 2006, doi/10.1895/wormbook.1.108.1

(30) Macleod, G. T.; Hegström-Wojtowicz, M.; Charlton, M. P.; Atwood, H. L. *J Neurophysiol* 2002, *88*, 2659.

(31) Macleod, G.; Marin, L.; Charlton, M.; Atwood, H. *J Neurosci* 2004, *24*, 2496.

(32) Ramachandran, P.; Budnik, V. *Cold Spring Harbor Protocols* 2010, *2010*, pdb.prot5469.

(33) Sulston, J.; Hodgkin, J. In *The Nematode Caenorhabditis elegans*; Wood, W., Ed.; Cold Spring Harbor Laboratory Press: New York, 1988, p 587.

(34) Yagi, H.; Kajiwara, N.; Tanaka, H.; Tsukihara, T.; Kato-Yamada, Y.; Yoshida, M.; Akutsu, H. *Proc Natl Acad Sci U S A* 2007, *104*, 11233.

(35) Ranganayakulu, G.; Elliott, D. A.; Harvey, R. P.; Olson, E. N. *Development* 1998, *125*, 3037.

(36) Thorat, L.; Gaikwad, S.; Nath, B. *Biochem Biophys Res Commun* 2012, *419*, 638.

(37) Morgan, P. G.; Kayser, E. B.; Sedensky, M. M. *WormBook : The online review of C. elegans biology*; The *C. elegans* Research Community Ed. 2007, doi/10.1895/wormbook.1.140.1

(38) Miro, O.; Barrientos, A.; Alonso, J. R.; Casademont, J.; Jarreta, D.; Urbano-Marquez, A.; Cardellach, F. *Eur J Clin Pharmacol* 1999, *55*, 35.

(39) Hertsens, R.; Jacob, W.; Van Bogaert, A. *Biochim Biophys Acta* 1984, *769*, 411.

(40) Dabadie, P.; Bendriss, P.; Erny, P.; Mazat, J. P. *FEBS Lett* 1987, *226*, 77.

(41) Rottenberg, H. *Proc Natl Acad Sci U S A* 1983, *80*, 3313.

(42) Cheng, A.; Wan, R.; Yang, J.; Kamimura, N.; Son, T.; Ouyang, X.; Luo, Y.; Okun, E.; Mattson, M. *Nat Commun* 2012, *3*, 1250.

(43) Li, Z.; Okamoto, K.; Hayashi, Y.; Sheng, M. *Cell* 2004, *119*, 873.

(44) Tsubouchi, A.; Tsuyama, T.; Fujioka, M.; Kohda, H.; Okamoto-Furuta, K.; Aigaki, T.; Uemura, T. *Development* 2009, *136*, 3757.

(45) Oruganty-Das, A.; Ng, T.; Udagawa, T.; Goh, E.; Richter, J. *Cell Metab* 2012, *16*, 789.

(46) Fu, D.; Mitra, K.; Sengupta, P.; Jarnik, M.; Lippincott-Schwartz, J.; Arias, I. *Proc Natl Acad Sci U S A* 2013, *110*, 7288.

(47) Lee, J.; Koh, H.; Kim, M.; Kim, Y.; Lee, S.; Karess, R.; Lee, S.; Shong, M.; Kim, J.; Kim, J.; Chung, J. *Nature* 2007, *447*, 1017.

(48) Brys, K.; Castelein, N.; Matthijssens, F.; Vanfleteren, J.; Braeckman, B. *BMC Biol* 2010, *8*, 91.

(49) Lee, I.; Hendrix, A.; Kim, J.; Yoshimoto, J.; You, Y. *PloS ONE* 2012, *7*, e44720.

(50) Rea, S. *Exp Gerontol* 2005, *40*, 841.

(51) Sahin, E.; DePinho, R. *Nat Rev Mol Cell Biol* 2012, *13*, 397.

(52) Vendelbo, M.; Nair, K. *Biochim Biophys Acta* 2011, *1813*, 634.

(53) Kanda, H.; Igaki, T.; Okano, H.; Miura, M. *Proc Natl Acad Sci U S A* 2011, *108*, 18977.

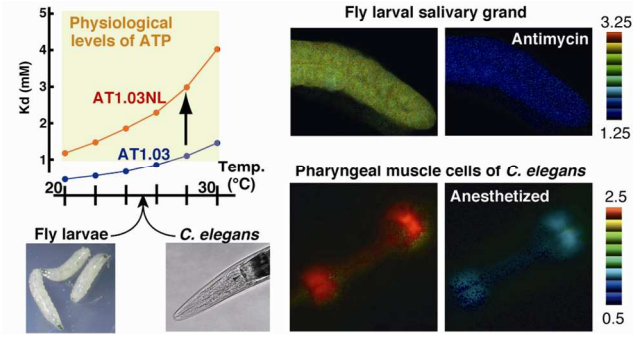
Physiological levels of ATP
Kd (mM)
AT1.03NL
AT1.03
Temp. (°C)
Fly larvae
C. elegans
Fly larval salivary grand
Antimycin
3.25
1.25
Pharyngeal muscle cells of C. elegans
Anesthetized
2.5
0.5

TOC only